APPLICATION OF FRICTION VELOCITY DETERMINATION TECHNIQUES TO NUMERICAL DATA OF MICRO VORTEX GENERATOR TURBULENT BOUNDARY LAYER

***Jiahao Kong*[1], *Bagus Nugroho*[2], *Luke G. Bennetts*[3], *Chi I. Chan*[1] *and Rey Chin*[1]**

[1] ***School of Electrical and Mechanical Engineering, University of Adelaide, South Australia 5005, Australia***

[2] ***Department of Mechanical Engineering, University of Melbourne, Melbourne, 3010 Victoria, Australia***

[3] ***School of Computer and Mathematical Sciences, University of Adelaide, South Australia 5005, Australia***

jiahao.kong@adelaide.edu.au

Abstract

Turbulent boundary layers controlled by miniature vortex generators (MVG-TBLs) remain unclear due to the lack of accurate friction velocity U_τ determination techniques, especially for experiments. This study investigated three U_τ-determination methods by applying those methods to large eddy simulation (LES) MVG data. The defect profile method cannot determine U_τ accurately at upstream locations with a short fitting range as the fitting range is insufficient to reflect the actual U_τ development. The modified Clauser chart method also defectively estimates U_τ with high uncertainty levels of $\geq 16\%$ at an upstream location due to the distortion of the linear log region. A method utilizing the inner-layer similarity and the modified Musker function is referred to as the inner method, which provides a good estimation of U_τ with uncertainty levels of $\leq 5\%$ even the LES MVG data removed from the near-wall measurements $y^+ < 12$. Therefore, the inner2 method is recommended for the U_τ determination from the streamwise velocity profiles of MVG TBLs.

1 Introduction

Micro vortex generators (MVGs) are used as a passive flow control to delay or prevent flow separation, which occurs when a fluid flows against an adverse pressure gradient (e.g., air flows over aircraft wings). The prevention of flow separation can improve energy efficiency by reducing pressure drag caused by the separation zone. The typical configuration of MVGs consists of pairs of triangular/rectangular blades mounted vertically in an array, orthogonal to the flow direction, on a flat plate. The mechanism of MVGs is to introduce streamwise vortices to re-energize the near-wall separated flow (Lin (1999)).

MVG flow control has been investigated experimentally and numerically for low-speed and supersonic laminar flows (Lin (1991) and Panaras et al. (2015)). An optimal MVG configuration suggested by Lin (1999) has MVGs with a device height (h) to boundary layer thickness (δ_0 at MVG position) ratio of $h/\delta_0 = 0.2$ in a counter-rotating arrangement, which can produce about 50% drag reduction for separated flows. MVGs are also under investigation in delaying laminar flows transitioning to turbulence, which can reduce friction drag by shifting the transition point downstream (Fransson (2006)). Sattarzadeh et al. (2014) reported that the net drag reduction achieves up to 65% when two arrays of MVGs are allocated at two streamwise locations to a transitioning flow.

MVG is also important for turbulent flows as it is observed to impose large-scale vortical motions in turbulent boundary layers (TBLs) (Chan and Chin (2022)) and explored for TBL flow control. The MVG TBLs have been investigated experimentally in terms of the MVG-induced streamwise vortices in the near-wall region (Lögdberg et al. (2009)). However, the investigation of the MVG TBLs remains limited as the lack of friction velocity U_τ determination techniques for MVG-TBL experiments.

Most friction velocity estimation techniques are based on the concept of wall similarity, which can be classified into three categories: outer-layer similarity, linear log-law, and inner-layer similarity. The defect profile method, based on the outer-layer similarity, is often used to determine U_τ for rough-wall TBLs (Kong et al. (2023)). The modified Clauser chart method (MCC) is based on the linear logarithm region and used to estimate U_τ for smooth- and rough-wall TBLs (Flack et al. (2007)). The composite method utilizing the modified Musker function (Musker (1979)) and the three wall similarity theories has been investigated in U_τ determination for smooth-wall TBLs (Rodríguez-López et al. (2015)). A method based on the inner-layer similarity and the modified Musker function can be developed for MVG-TBL flows as the MVG-influenced velocity profiles show

the collapsing viscous layer (Chan and Chin (2022)), which is referred to as the 'inner' method in the present study. The large eddy simulation (LES) MVG result of Chan and Chin (2022) also shows the linear log-law region and support of the outer-layer similarity. To the best knowledge of the authors, few MVG experimental studies have applied the wall-similarity methods to determine U_τ (Ye et al. (2016)). There is a need to examine the U_τ-determination methods and develop an appropriate technique for MVG-TBL experiments.

The present study aims at investigating the performance of U_τ-determination of the three techniques for MVG-influenced TBLs, including the defect profile, modified Clauser chart, and inner methods. The applications of the three methods are performed to the LES MVG database of Chan and Chin (2022), and different combinations of the fitting ranges are investigated to develop the optimal fitting range for each technique. Then the performance of the three techniques is examined again by applying them to the data-missing LES MVG database to mimic the experimental limitations of the missing near-wall measurements.

2 Friction velocity estimation techniques description

The defect profile method is based on the outer-layer similarity hypothesis, stating that the outer layer is unaffected by the wall condition at a sufficiently large Reynolds number (Townsend (1976)) and follows a universal defect law as equation,

$$\frac{U_\infty - U}{U_\tau} = -\frac{1}{\kappa}\ln\left(\frac{y}{\delta}\right) + \frac{\Pi}{\kappa}\left[w(1) - w(\frac{y}{\delta})\right]. \quad (1)$$

where U_∞ is free-stream velocity, κ is the von Kármán constant, and w is the wake function. The procedure is as follows: an inner-scaled defect profile is obtained from a smooth-wall TBL first. Then the measured data $U_\infty - U$ in MVG-influenced flows is fit onto the reference profile by adjusting U_τ. The U_τ is determined when the fitting error reaches the least square error.

The Clauser chart method, proposed by Clauser (1954), was the first to utilize the log layer to determine U_τ for smooth-wall TBLs as,

$$\frac{U}{U_\tau} = \frac{1}{\kappa}\ln\left(\frac{yU_\tau}{\nu}\right) + C, \quad (2)$$

where $C = 5.3$ is an additive constant for the smooth-wall TBL and ν is the kinetic viscosity. Perry and Li (1990) developed the modified Clauser method (MCC) from the velocity defect law in the log-law layer part (see Eq.1). The equation of the MCC method is,

$$\frac{U}{U_\infty} = 1 + \frac{1}{\kappa}\frac{U_\tau}{U_\infty}\ln\left(\frac{y}{\delta^*}\right) + \frac{1}{\kappa}\frac{U_\tau}{U_\infty}\left[\ln\left(\frac{U_\tau}{U_\infty}\right) + \ln\left(\frac{1+\Pi}{\kappa}\right)\right] - \frac{U_\tau}{U_\infty}\frac{2\Pi}{\kappa}, \quad (3)$$

where δ^* is the displacement thickness. This method plots all measured data as U/U_∞ vs $\ln(y/\delta^*)$. The data points in the fitting range $y/\delta^* = 0.25$–0.9 were compared with a family of linear constant lines with slopes of $\frac{1}{\kappa}\frac{U_\tau}{U_\infty}$ for smooth-wall TBLs. The friction velocity is obtained when the fitting between constant lines and the log-law data points reaches the least square error. Perry and Li (1990) found that this method can estimate U_τ within a $\pm 3\%$ error.

The inner method is based on the modified Musker function. Musker (1979) developed an adaption function of the buffer layer to asymptotically connect the viscous sublayer and the linear log law layer to describe the inner layer. Monkewitz et al. (2007) developed the modified Musker function with an additional 'hump' function, which results in better agreement with the smooth-wall experimental data in the buffer layer. The modified Musker function is given as,

$$U^+_{\text{Musker}} = \frac{1}{\kappa}\ln\left(\frac{y^+ - a}{-a}\right) + \frac{R^2}{a(4\alpha - a)} \times \left[(4\alpha + a)\ln\left(-\frac{a}{R}\frac{\sqrt{(y^+ - \alpha)^2 + \beta^2}}{y^+ - a}\right) + \frac{\alpha}{\beta}(4\alpha + 5a)\left(\arctan(\frac{y^+ - \alpha}{\beta}) + \arctan(\frac{\alpha}{\beta})\right)\right] + \frac{\exp\left[-\ln^2(y^+/30)\right]}{2.85}, \quad (4)$$

where $\alpha = (-1/\kappa - a)/2$, $\beta = \sqrt{-2a\alpha + \alpha^2}$, $R = \sqrt{\alpha^2 + \beta^2}$. The superscript $+$ indicates the scaling of viscous units, namely the friction velocity U_τ and the viscous length $l_v = \nu/U_\tau$, for instance, $y^+ = yU_\tau/\nu$. The key feature of this function is that the parameter a can be adjusted to output various combinations of κ and additive constant C in Eq 2. The von Kármán constant is suggested as $\kappa = 0.41$ (Chan and Chin (2022)). Hence, U^+_{Musker} is a function of U_τ, and κ.

This study employs an optimization technique to determine the parameters of U_τ and constant a, which is similar to that of Rodríguez-López et al. (2015). The optimization mainly comprises the problem function, optimization problem definition and the optimization algorithm. The error function is defined as,

$$E(U_\tau, a) = \frac{|U^+_{\text{Musker}}(U_\tau,\ a) - U^+_{measured}(U_\tau)|}{U^+_{\text{Musker}}(U_\tau,\ a)} \quad (5)$$

$U^+_{measured}$ is the target profile from the experimental measurement. The optimization problem can be described as follows,

$$\text{find min}[E(U_\tau,\ a)],$$
$$\text{subject to} \begin{cases} U_\tau \in [U_{\tau,min}\ , U_{\tau,max}] \\ a \in [a_{,min},\ a_{,max}]. \end{cases}$$

The bounds of two variables are set to increase the robustness of this technique. The bounds are selected to be far enough from the optimal results after each optimization to ensure the optimization process is not affected by the bounds. The initial $U_{\tau,i}$ is determined by the defect profile method and the initial a_i is -10.58, which yields $\kappa = 0.41$ and $C = 5.2$ for smooth-wall TBLs. The optimization problem can be rewritten as the Lagrangian problem as $\mathcal{L}(\boldsymbol{x_k}, \boldsymbol{\lambda}) = E(\boldsymbol{x_k}) - \boldsymbol{\lambda}^T \boldsymbol{b}(\boldsymbol{x_k})$, where E is the error function (Eq 5), $\boldsymbol{x_k}$ are the optimized variables, $\boldsymbol{b}$ are the bounds of two variables, and $\boldsymbol{\lambda}$ are the Lagrange multiplicators. The optimization problem is solved using sequential quadratic programming and a quadratic subproblem (Nocedal and Wright (2006)). The sequential quadratic programming will be implemented with a MATLAB function *fmincon*. The tolerances of variables $\boldsymbol{x_k}$ and the error function E are set to 10^{-10}.

3 Database Detail and MVG configuration

The LES MVG database is obtained by a well-resolved large-eddy simulation with a domain in the streamwise, wall-normal and spanwise directions, respectively: $x_L \times y_L \times z_L = 6000\delta_0^* \times 200\delta_0^* \times 360\delta_0^*$ (δ_0^* is inlet the displacement thickness), giving grid spacings of $\Delta x^+ \approx 16.9$ and $\Delta z^+ \approx 8.1$ in the streamwise and spanwise directions. The wall-normal data points start from the wall at $y^+ = 0.03$.

The MVG configuration and geometry are shown in Figure 1. A total of seven pairs of MVG were spanwisely placed at $x_M/\delta_0^* = 950$, corresponding to $Re_\tau \approx 430$. x^* is the streamwise distance downstream of the MVG array, $x^* = x - x_M$. The boundary layer thickness δ is defined at which the velocity reaches $U/U_\infty = 0.99$ and δ_0 is the boundary layer thickness at $x = x_M$. The LES MVG database is provided by the flow field measurements of a total 429 linear-spaced spanwise positions within $-2.5\Lambda_z \le z \le 2.5\Lambda_z$ at five streamwise locations of $x^*/h = 5$, 25, 50, 200, and 500.

The global velocity profile and friction velocity of each streamwise location were obtained by averaging 429 spanwise velocity profiles and U_τ values, respectively. The global boundary layer condition detail is summarized in Table 1. The global U_τ and skin friction coefficient c_f reduce along the streamwise development. The friction Reynolds number Re_τ develops up to ≈ 950 at $x^*/h = 500$.

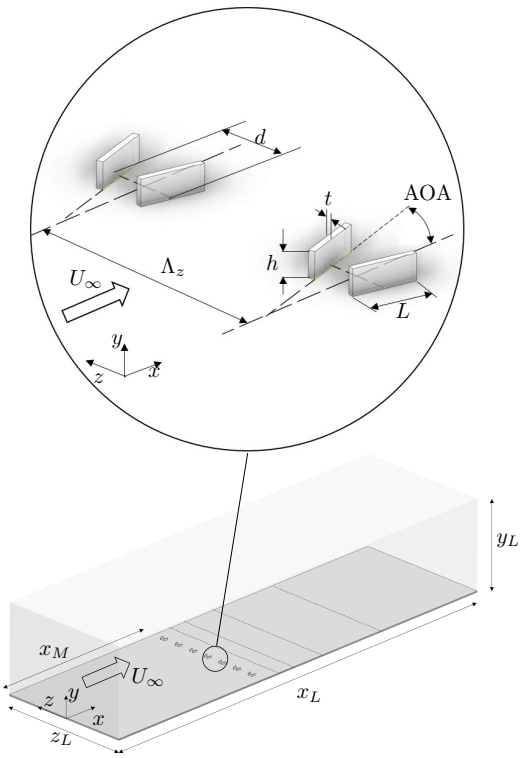

Figure 1: Schematic views of flow domains and MVG configuration.

Table 1: Boundary condition detail of the LES MVG database (Chan and Chin (2022)). The thickness parameters are scaled with δ_0^*.

x^*/h	δ	θ	δ^*	H	U_τ	$1000c_f$	Re_τ
5	21.86	2.77	4.18	1.51	0.0458	4.23	451
25	23.21	2.95	4.34	1.47	0.0444	3.93	468
50	24.80	3.15	4.60	1.46	0.0437	3.80	496
200	34.39	4.24	6.03	1.42	0.0423	3.58	660
500	52.28	4.31	6.12	1.42	0.0403	3.25	948

4 Result and discussion

This study utilized the global velocity profile and the three proposed techniques to determine the global U_τ, where the estimated U_τ is also compared with the true U_τ, provided in Table 1. The performance of the defect profile method varies with different fitting ranges. Here, the fitting ranges span over combinations of $0.1 \le y_I/\delta \le 0.6$ and $0.8 \le y_O/\delta \le 1.2$. y_I and y_O are the inner and outer bounds of the fitting range. The estimated U_τ of the defect profile method is compared with the true U_τ of the LES MVG case and plotted in the form of a contour map of $E_{U_\tau}(\%) = \frac{U_\tau|_{\text{esti}} - U_\tau|_{\text{true}}}{U_\tau|_{\text{true}}} \times 100$, as shown in Figure 2.

The result shows that the estimation of the defect profile method is insensitive to the outer bound. The red circle indicates a fitting range showing low-error levels of $E_{U_\tau} < 3\%$ at $x^*/h \geq 25$. This output indicates the range of $y/\delta = 0.6$–1 is suggestive as the universal fitting range for the defect method at $x^*/h \geq 25$ with low uncertainty levels of $< 3\%$. But the defect method shows a high uncertainty of $E_{U_\tau} \approx 6\%$ by applying the universal fitting range, which is due to the velocity deficits induced by MVGs (Chan and Chin (2022)).

The performance of the modified Clauser chart

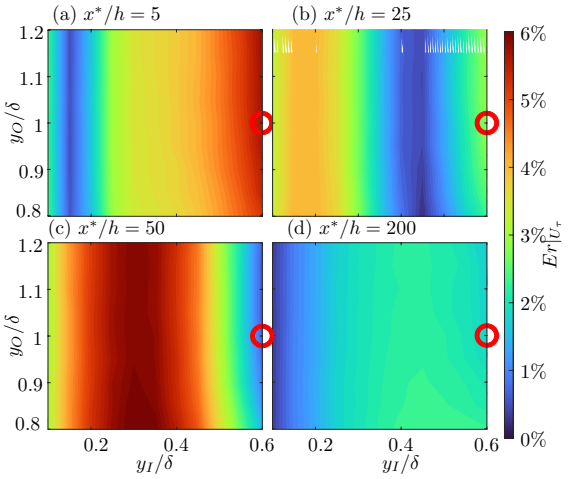

Figure 2: The mean relative error distribution with varying fitting ranges generated by the defect profile method at $x^*/h = 5$, 25, 50, and 200. The red circle refers to the fitting range generating the low error at $x^*/h \geq 25$.

method (MCC) depends on the accurate definition and the thickness of the log-law layer (Walker (2014)). The log region bounds are defined with the scaling of the displacement thickness δ^* for the MCC method. The inner bound range is selected from the wall of $y_I/\delta^* = 0.01$ to 0.57. The outer bound range is chosen from $y_O/\delta^* = 0.58$ to $3\delta^*$. The friction velocity error distribution is plotted in Figure 3. The MCC method shows a deficiency of U_τ estimation with uncertainty levels of $\geq 12\%$ at $x^*/h = 5$ (Figure 3a). Figures 3(b–e) show a similar error distribution, which suggests that the MCC method defectively estimates U_τ with a large error of $E_{U_\tau} > 10\%$ when the inner bound $y_I/\delta^* < 0.15$ at $x^*/h = 25$–500. The outer bound is suggested to be $y_O/\delta^* > 1.2$ to keep the error $E_{U_\tau} < 10\%$. The error reduces with a higher inner bound. A universal fitting range is indicated by the red circle from $y_I/\delta^* = 0.27$ to $y_O/\delta^* = 1.445$, which is applied with the MCC method and produce an accurate U_τ-estimation with uncertainty levels of $< 3\%$ at $x^*/h = 25$–500.

The inner method naturally provides better performance on U_τ estimation with closer near-wall measurement. The inner bound of the fitting range should start from the lowest wall-normal position y^+_{min}. However, due to the experimental limitations of the missing near-wall measurements, it is necessary to investigate the impact of various inner bounds of the fitting ranges to mimic the limitations of missing near-wall measurements. The outer bounds are investigated to define the optimal outer bound for different starting points of the fitting range. The inner bound range is selected from the wall to $y^+_I = 60$, slightly below the buffer layer's top bound at $y^+ = 70$ (Marusic et al. (2010)). The conservative outer bound range is chosen as $y^+_O/\sqrt{Re_\tau} = 1$–20 ($y_O/\delta \approx 0.02$–0.3), which can fully cover the suggestive log region for the smooth-wall TBL, which is from $y^+_I/\sqrt{Re_\tau} = 2.5$ to $y_O/\delta = 0.15$.

The resultant friction velocity is compared with the true U_τ, and the U_τ error map is plotted in Figure 4. Figure 4(a) shows that the estimation error is less than 3% when using an inner bound $y^+_I \leq 5$ at $x^*/h = 5$ and 25. With this inner bound, the U_τ estimation is insensitive to the outer bound; even when the outer bound spans over a range to $y^+ = 20\sqrt{Re_\tau}$. For $y^+_I \geq 12$, the U_τ error increases to higher than 10% coupled with choosing an outer bound $y^+_O/\sqrt{Re_\tau} \geq 4$ at $x^*/h = 5$ and 25. For downstream locations $x^*/h \geq 50$ (Figures 4b–e), the low error area ($E_{U_\tau} \leq 3\%$) becomes larger than that of $x^*/h = 5$ and 25, which indicates that the inner method shows an excellent capability to estimate U_τ after $x^*/h \geq 50$ accurately. A universal fitting range with a low estimation error $E_{U_\tau} \leq 3\%$ can be achieved with an inner bound, $y^+_I \leq 12$ and an outer bound, $y^+_O/\sqrt{Re_\tau} = 2$. The limit of the inner bound is achievable for TBL experiments (Kong et al. (2023)).

The three proposed methods are applied to the limited LES MVG database using the above-investigated universal fitting ranges at $x^*/h = 5$–500. The limited LES MVG database is excluded from the near-wall measurements of $y^+ < 12$. For the defect profile method, the applied fitting range is $y_I = 0.6\delta$ to $y_O = 1\delta$. The fitting range for the MCC method is $y_I = 0.27\delta^*$ to $y_O = 1.445\delta^*$. As the limited LES MVG profile starts from $y^+ = 12$, the fitting range for the inner method is chosen from $y^+_I = 12$ to $y^+_O = 2\sqrt{Re_\tau}$

The resultant U_τ and the difference between the estimated U_τ and the true U_τ from the LES MVG database are summarized in Table 2. The U_τ values of the defect profile method remain nearly constant along the streamwise development, which does not reflect the influence caused by MVGs. Therefore, the defect method is insensitive to the MVGs influence and cannot determine U_τ accurately by applying a universal fitting range of $y/\delta = 0.6$–1 at $x^*/h \leq 50$. However, the defect method provides a rough esti-

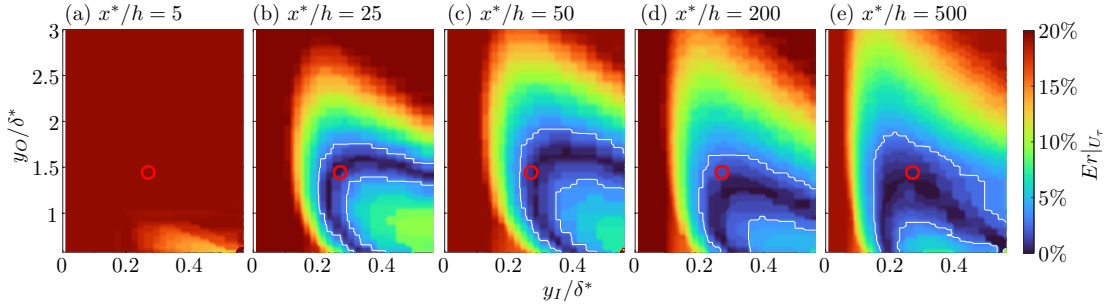

Figure 3: The mean relative error distribution with varying fitting ranges generated by the MCC method. Solid iso-line refers to the level of 3%. The red circle located within the iso-line area ($E_{U_\tau} < 3\%$) indicates the optimum fitting range at $x^*/h = 25$–500.

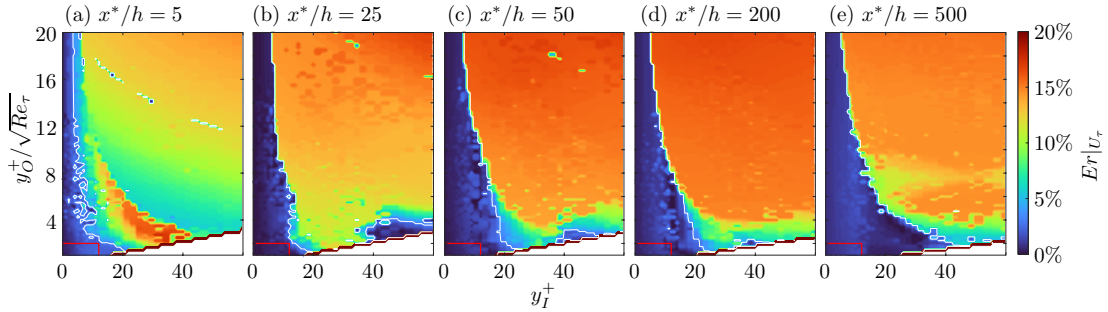

Figure 4: The mean relative error distribution with varying fitting ranges generated by the inner method. Solid iso-line refers to the level of 3%. The red box located within the iso-line area ($E_{U_\tau} \leq 3\%$) indicates the optimum fitting ranges at $x^*/h = 5$–500.

Table 2: Friction velocity values estimated from the three proposed methods with improved fitting range for the data-missing LES MVG database. The LES MVG data is excluded for the near-wall data points $y^+ < 12$. The error between the estimated and true value at five locations, $x^*/h = 5$, 25, 50, 200, 500. The values of LES MVG refer to the true U_τ. U_τ is scaled with U_∞.

x^*/h	5		25		50		200		500	
Method	U_τ	$E_{U_\tau}(\%)$	U_τ	$E_{U_\tau}(\%)$	U_τ	$E_{U_\tau}(\%)$	U_τ	$E_{U_\tau}(\%)$	U_τ	$E_{U_\tau}(\%)$
Defect	0.0434	-5.7	0.0431	-2.9	0.0439	0.7	0.0431	1.9	-	-
MCC	0.0537	16.9	0.0437	-1.4	0.0446	2.3	0.0430	1.6	0.0403	-0.1
inner	0.0448	-2.5	0.0452	1.8	0.0434	-0.5	0.0423	0.1	0.0399	-1.2
LES MVG	0.0458	-	0.0444	-	0.0437	-	0.0423	-	0.0403	-

mation of U_τ with an uncertainty of $\approx 6\%$ for five streamwise positions. The MCC method defectively estimates U_τ with $E_{U_\tau} > 16\%$ at $x^*/h = 5$ due to the log-law layer distortion. However, the MCC method shows a good performance in estimating U_τ with $E_{U_\tau} < 3\%$ at $x^*/h \geq 25$ as the log-law region starts to redevelop at $x^*/h \geq 25$. The inner method shows better performance than the other methods. The estimation error is less than 3% at $x^*/h \geq 5$, within the acceptable range (Flack et al. (2007)). Hence, the inner method is recommended for the U_τ determination of the MVG-TBL experiments can obtain the velocity profile down to $y^+ = 12$.

5 Conclusions

The friction velocity U_τ is vital in analyzing turbulent boundary layers, particularly for TBLs influenced by flow control techniques, e.g., MVGs. Some natures of the smooth-wall TBLs may be modified due to the MVG-induced vortices, including the linear log-law layer and the outer layer similarity (Ye et al. (2016)). This study investigated three techniques based on the outer-layer similarity, linear log law and the inner layer similarity to determine U_τ for MVG TBLs. The performance of the five proposed methods was examined by applying those methods to the LES MVG database of Chan and Chin (2022).

The defect profile method is unable to determine U_τ using the fitting range of $y/\delta = 0.6$–1 at $x^*/h \leq 200$ as the fitting range is too short to reflect the actual friction velocity. The modified Clauser chart method (Perry and Li (1990)) shows a

deficiency in U_τ estimation with a high uncertainty level of $\geq 16\%$ at $x^*/h = 5$ due to the log-law layer distortion. For the downstream locations $x^*/h \geq 25$, the MCC method can achieve a low level of U_τ error of $\leq 2\%$ for the LES MVG database as the log-law region starts to redevelop. The inner method provides better performance in estimating U_τ as the uncertainty can be maintained at less than 3% for the whole range of streamwise positions of $x^*/h \geq 5$, and this method is recommended for the U_τ determination of MVG-TBL experiments as the inner bound limit of the fitting range is achievable for TBL experiments.

Acknowledgments

The authors wish to thank the Australian Research Council (ARC) for the financial support for this research.

References

J. C. Lin (1999), Control of turbulent boundary-layer separation using micro-vortex generators, 30th Fluid Dynamics Conference, 10.2514/6.1999-3404.

J. Lin, F. Howard, and G. Selby (1991), Exploratory study of vortex-generating devices for turbulent flow separation control, in 29th Aerospace Sciences Meeting (AIAA).

A. G. Panaras and F. K. Lu (2015), Micro-vortex generators for shock wave/boundary layer interactions," Progress in Aerospace Sciences 74, 16–47.

J. H. Fransson, A. Talamelli, L. Brandt, and C. Cossu (2006), Delaying transition to turbulence by a passive mechanism, *Physical Review Letters* 96, 1–4.

S. S. Sattarzadeh, J. H. Fransson, A. Talamelli, and B. E. Fallenius (2014), Consecutive turbulence transition delay with reinforced passive control, *Physical Review E - Statistical, Nonlinear, and Soft Matter Physics* 89, 061001.

C. Chan and R. Chin (2022), Investigation of the influence of miniature vortex generators on the large-scale motions of a turbulent boundary layer, *Journal of Fluid Mechanics* 932, A29.

O. Lögdberg, J. H. Fransson, and P. H. Alfredsson (2009), Streamwise evolution of longitudinal vortices in a turbulent boundary layer, *Journal of Fluid Mechanics* 623, 27–58.

J. Kong, L. G. Bennetts, B. Nugroho, and R. C. Chin (2023), Systematic study of the Reynolds number and streamwise spacing effects in two-dimensional square-bar rough-wall turbulent boundary layers, *Physical Review Fluids* 8, 014601.

K. A. Flack, M. P. Schultz, and J. S. Connelly (2007), Examination of a critical roughness height for outer layer similarity, *Physics of Fluids* 19, 95104.

A. J. Musker (1979), Explicit expression for the smooth wall velocity distribution in a turbulent boundary layer, AIAA Journal 17, 655–657.

E. Rodríguez-López, P. J. Bruce, and O. R. Buxton (2015), A robust post-processing method to determine skin friction in turbulent boundary layers from the velocity profile, *Experiments in Fluids* 56, 68.

Q. Ye, F. F. Schrijer, and F. Scarano (2016), Boundary layer transition mechanisms behind a micro-ramp, *Journal of Fluid Mechanics* 793, 132–161.

A. A. Townsend (1976), The structure of turbulent shear flow, 2nd ed., (Cambridge University Press, Cambridge, England; New York, 1974) p. 429.

F. H. Clauser (1954), Turbulent boundary layers in adverse pressure gradients, *Journal of the Aeronautical Sciences* 21, 91–108.

A. E. Perry and J. D. Li (1990), Experimental support for the attached-eddy hypothesis in zero pressure-gradient turbulent boundary layers, *Journal of Fluid Mechanics* 218, 405–438.

P. A. Monkewitz, K. A. Chauhan, and H. M. Nagib (2007), Self-consistent high-Reynoldsnumber asymptotics for zero-pressure-gradient turbulent boundary layers, *Physics of Fluids* 19, 115101.

J. Nocedal and S. J. Wright (2006), Numerical optimization, Springer Series in Operations Research and Financial Engineering, 1–664.

J.M.Walker (2014), The application of wall similarity techniques to determine wall shear velocity in smooth and rough wall turbulent boundary layers, *Journal of Fluids Engineering*, 136, 051204.

K. A. Flack, M. P. Schultz, and J. S. Connelly (2007), Examination of a critical roughness height for outer layer similarity, *Physics of Fluids* 19, 95104.

I. Marusic, B. J. McKeon, P. A. Monkewitz, H. M. Nagib, A. J. Smits, and K. R. Sreenivasan (2010), Wall-bounded turbulent flows at high Reynolds numbers: Recent advances and key issues, *Physics of Fluids* 22, 1–24.